Implementation of Linear Filters for Iterative Penalized Maximum Likelihood SPECT Reconstruction [1)]

Zhengrong Liang
Department of Radiology, Duke University Medical Center
Durham, North Carolina 27710

Abstract

Six low-pass linear filters applied in frequency space were implemented for iterative penalized maximum-likelihood (ML) SPECT image reconstruction. The filters implemented were the Shepp-Logan filter, the Butterworth filter, the Gaussian filter, the Hann filter, the Parzen filter, and the Lagrange filter. The low-pass filtering was applied in frequency space to projection data for the initial estimate and to the difference of projection data and reprojected data for higher order approximations. The projection data were acquired experimentally from a chest phantom consisting of non-uniform attenuating media. All the filters could effectively remove the noise and edge artifacts associated with ML approach if the frequency cutoff was properly chosen. The improved performance of the Parzen and Lagrange filters relative to the others was observed. The best image, by viewing its profiles in terms of noise-smoothing, edge-sharpening, and contrast, was the one obtained with the Parzen filter. However, the Lagrange filter has the potential to consider the characteristics of detector response function.

I. INTRODUCTION

Quantitative single photon emission computed tomography (SPECT) has been limited mainly by the inadequate number of detected photons in projections. The projection data contain Poisson noise associated with photon detection, attenuation and scattering effects of photons within the patient body, and the variations in collimator response with distance. The iterative maximum-likelihood, expectation-maximization (ML-EM) algorithm [1,2] provides a simple and accurate formula to compensate these effects. Although the ML-EM algorithm can incorporate these effects in the SPECT reconstruction (as well as the non-negativity of image pixel values and the conservation of the acquired data), its neglect of correlations among nearby pixels may cause the noise and edge artifacts in the reconstructed images [3]. Moreover, the compensation during the reprojection and backprojection processes of the ML-EM algorithm is time consuming. The objective of this research was to implement the low-pass smoothing filters applied in frequency space [4,5] to alleviate the artifacts and reduce the computation time.

1) This work was supported by Grant #HL44194, awarded by the National Heart, Lung, and Blood Institute, and in part by Grant #CA33541, awarded by the National Cancer Institute and by Grant #DEFG05-89ER60894, awarded by the Department of Energy.

II. THEORY

The log likelihood of a Poisson distributed photon-detection process is well known [1-3]:

$$L(\mathbf{Y}\,|\,\Phi)=\sum_i [\,-\sum_j R_{ij}\,\phi_j + Y_i\,ln\,(\sum_j R_{ij}\,\phi_j) - ln\,(Y_i!)\,] \qquad (1)$$

where $\mathbf{Y} = \{Y_i\}_{i=1}^{I}$ is the data vector with I elements, $\Phi = \{\phi_j\}_{j=1}^{J}$ is the image vector of J elements to be reconstructed, and R_{ij} is the probability of detecting a photon emitted within pixel j and registered at detector bin i. In SPECT, the value of R_{ij} depends on the deterministic effects of pixel-projection geometry, photon attenuation and scattering, and collimation variations [6]. By use of Stirling's approximation, the likelihood function (1) becomes:

$$L(\mathbf{Y}\,|\,\Phi)=\sum_i [\,-Y_i\,ln\,(Y_i/\sum_j R_{ij}\,\phi_j\,)+(Y_i-\sum_j R_{ij}\,\phi_j)\,]. \qquad (2)$$

This is the Kullback-Leibler information criterion [7] and has been widely used in information theory.

It has been recognized that the ML criterion [Eq.(1) or (2)] has the intrinsic instability of generating noisier images as the likelihood increases at higher iterations [3]. This instability associated with ML approach may be due to the neglect of the correlations among nearby pixels. A formal way to impose the correlations upon the ML approach is to carry out the maximum *a posteriori* probability (MAP) criterion by specifying an *a priori* probability reflecting the correlations via Bayesian analysis.

Let the log *a priori* probability of the correlations among nearby pixels be $H(\Phi)$, the log *posteriori* probability is then:

$$g(\Phi) = L(\mathbf{Y}\,|\,\Phi) + H(\Phi)\,. \qquad (3)$$

Following the derivations given in [8], the solution which maximizes $g(\Phi)$ is determined iteratively by:

$$\phi_k^{(n+1)} = \phi_k^{(n)}\,\frac{\sum_i R_{ik}\,(\,Y_i/\sum_j R_{ij}\,\phi_j^{(n)}\,)}{\sum_i R_{ik}\,[\,1+\xi_k^{(n)}\,Z_k(\Phi^{(n)})\,]} \qquad (4)$$

$$= \bar{\phi}_k^{(n)}\,\frac{\sum_i R_{ik}\,(\,Y_i/\sum_j R_{ij}\,\phi_j^{(n)}\,)}{\sum_i R_{ik}} \qquad (5)$$

where $Z_k = \partial H(\Phi)/\partial\phi_k$, $\xi_k^{(n)}$ is an adjustable parameter, and $\bar{\phi}_k^{(n)} = \phi_k^{(n)}/(1+\xi_k^{(n)}\,Z_k)$ is the smoothed value of pixel k. The smoothing for $\bar{\phi}_k^{(n)}$ is determined by the assumed *a priori* correlations Z_k among nearby pixels.

The difficulties with this formal MAP approach are the specifications of an adequate prior Z_k and the adjustable parameter $\xi_k^{(n)}$. If an inadequate prior or adjustable parameter

0018-9499/91/0400-0606$01.00 © 1991 IEEE

is used, artificial biases and distortions are very likely to be generated in the reconstructed images [8]. Research for adequate priors and appropriate numerical methods has been an interesting topic in recent years [9-11].

Perhaps an easier approach to penalize the ML estimation is to use spatial-domain, non-linear smoothing techniques [12]. The non-linear smoothing can be easily used to determine the $\bar{\phi}_k^{(n)}$ in Eq.(5). When applying this spatial-domain penalized ML approach of Eq.(5) to SPECT reconstruction, the computation burden for R_{ik} (which contains attenuation, scattering, and collimation variation effects) during the reprojection and backprojection processes is very heavy. One way to reduce the computation time is to cut the compensating calculations during the backprojection using the filtered backprojection approach [5]. Keeping this in mind, equation (5) can be reformed as:

$$\phi_k^{(n+1)} = \bar{\phi}_k^{(n)} + \frac{\sum_i [R_{ik}\,\bar{\phi}_k^{(n)} / \sum_j R_{ij}\,\phi_j^{(n)}]\,(Y_i - \sum_j R_{ij}\,\phi_j^{(n)})}{\sum_i R_{ik}} \quad (6)$$

where the first term on the right-hand side (RHS) is the smoothed estimate at the n-th iteration and the second term is the correction for the $(n+1)$th approximation. The term in the bracket of Eq.(6) represents the ratio of the contributions of a group of pixels around pixel k and all pixels to the acquired datum Y_i. The ratio $T_{ik} = R_{ik}\,\bar{\phi}_k^{(n)} / \sum_j R_{ij}\,\phi_j^{(n)}$ depends on the source distribution (R_{ik} and Φ) and the *a priori* information about the smoothing associated with $\bar{\phi}_k^{(n)}$.

An assumption is made that the ratio T_{ik} represents a convolution operator. Mathematically the assumption is expressed as $T_{ik} = T(i-k)$. This assumption is heuristc. Detailed discussion is beyond this paper. Since the smoothing in image space is desired for the convolution operator, the corresponding operator in frequency space would be a low-pass filter [4-5]. Since the mapping of the smoothing from image space to projection space is very difficult to formulated mathematically, the expression of the low-pass filter with the desired smoothing property is not known yet. In this paper, those low-pass filters of well known characteristics [4-5] are considered and compared for the purpose of alleviating the artifacts associated with the ML-EM algorithm.

It is noted that a similar filtering approach has been taken by Tanaka [13-15] to improve the performance of the ML-EM algorithm. Tanaka introduced two convolution operators of Eq.(20) in [13] to adjust the ratio of projection data and reprojected data $\{Y_i / \sum_j R_{ij}\,\phi_j^{(n)}\}$ at each iteration. Substantial variations along the approach are presented in [15].

III. METHODS

Six low-pass linear filters applied in frequency space were implemented to filter the frequency components of $\{Y_i - \sum_j R_{ij}\,\phi_j^{(n)}\}$ in the second term on the RHS of Eq.(6) for the iterative penalized ML-EM algorithm (6). The filters implemented were the Shepp-Logan filter [16], the Butterworth filter [4], the Gaussian filter [17], the Hann filter [4], the Parzen filter [18], and the Lagrange filter [19]. These filters are defined, in the field of reconstruction from projections, by the corresponding windows multiplied by the ramp function $|f|$ (f is the spatial frequency) [5]. The former five windows were described in detail in [5]. The Lagrange window is defined as:

$$F(f) = \frac{1}{1 + \eta\,(2\pi f)^4 / |MTF(f)|^2} \quad (7)$$

where η is a parameter and $MTF(f)$ is the Fourier transform of the detector response function. The value $\eta \approx 5$ was used. $MTF(f) = exp[-(1/2)(f/f_N)^2]$ was assumed [20]. f_N is the Nyquist frequency. In the implementation, f_N was defined by the unit of *cycles / pixel* and $f_N = 0.5$ was then chosen.

The parameter $(2n)$ defined in the Butterworth window, $1/[1+(f/f_N)^{2n}]$, was chosen to be 20 [5]. (When $2n = 8$ was used, the resulting images were similar to those with $2n = 20$). For the Gaussian window, $exp[-\pi (f/\sigma)^2]$ with $\sigma = 4\,ln(2)/\pi\,(FWHM)^2$, the parameter of full-wide-half-maximum ($FWHM$) relating to detector resolution was assumed to be 2 [5]. (When value 4 was used, similar results were obtained). The parameter values chosen above have been widely used, e.g., see [5,16-20]. There is no parameter in the other three windows.

Two approaches in image space were used to calculate the first term $\bar{\phi}_k^{(n)}$ on the RHS of Eq.(6): one assumed a very weak correlation among nearby pixels (i.e., $\bar{\phi}_k^{(n)} \Rightarrow \phi_k^{(n)}$), another used the edge-preserving smoothing [21] for a relatively strong correlation.

The initial estimate $\Phi^{(0)}$ was computed as follows [see Eq.(5)]: First apply the chosen low-pass filter in frequency space to filter the acquired data $\{Y_i\}$ and then backproject the filtered data to image space. [The filtering and backprojection are the well known filtered backprojection method (FBP)]. Finally the backprojected image was divided by the normalization factors $\{\sum_i R_{ik}\}$. In the implementation, these factors contain the information about the geometry between pixels and projections and the non-uniform attenuating properties of a chest phantom from which the data were acquired. The negative pixel values were either accepted or forced to be zero for higher order approximations. This will be discussed later.

A fast non-uniform attenuated projector was used in computing the reprojected data $\{\sum_j R_{ij}\,\phi_j^{(n)}\}$ and the normalization factors $\{\sum_i R_{ik}\}$. The fast attenuated projector is similar to the one described in [22]. The differences between them are: (i) the attenuation factor within each pixel is calculated by mass-center average in the fast projector and by integral in [22]; and (ii) the intersecting lengths of pixels and projection rays are computed by recursion in the fast projector and by forward tracing in [22]. As an example of projecting a 128×128 image array to 120 projections with 128 sam-

ples per projection, the fast attenuated projector took 33 *seconds* to finish the projecting process, while the projector of [22] needed 58 *seconds*. The 2-point interpolation backprojector [23] was used to backproject the filtered data $\{T_{ik}\, Y_i\}$ for the initial estimate and $\{T_{ik}\,(Y_i - \sum_j R_{ij}\,\phi_j^{(n)})\}$ for higher order approximations. Since the compensation of non-uniform attenuation was not involved in the backprojection, less computation time was needed. The interpolation backprojector uses the distance between the pixel center and the projection ray as the weight rather than the intersection length of the pixel and the projection ray (as the attenuated projector does).

The chest phantom with non-uniform attenuating properties was an elliptical cylinder filled with water containing I^{123}. Within the elliptical cross section there were two regions of low density wood "lungs" and a region of nylon "bone" as shown by Fig.1. Both the lung and bone regions had zero activity. A hot sphere within the cylinder had approximately five times the concentration of I^{123} as the water had. The non-uniform attenuating properties of the phantom were considered during image reconstruction process.

The projection data were acquired at 120 projection angles equally spaced over 360 degrees by a three-headed SPECT system[2] with medium energy, parallel hole collimators. Each projection had 128×128 samples equally spaced. The projection slice through the center of the hot sphere had approximately half million counts and was used to reconstruct the 128×128 image array. Detailed information can be found in [24].

The attenuation map of the chest phantom was obtained by the uncompensated reconstruction from the acquired data and the known attenuation coefficients of the phantom.

The evaluations at the performance of the low-pass linear filters were based on the horizontal and vertical profiles through the reconstructed images. The profiles were examined, by viewing, in terms of noise-smoothing, edge-sharpening, and contrast between the regions of the lung, bone, hot sphere, and background.

IV. RESULTS

In this section, a few typical images reconstructed by applying the penalized ML-EM algorithm (6) to the acquired data from the chest phantom are presented. The profiles shown were drawn through the images at the positions indicated. The difference of smoothing the first term $\bar{\phi}_k^{(n)}$ on the RHS of Eq.(6) with weak and strong correlations will be reported. The effect of accepting negative pixel values or forcing them to be zero for higher order approximations will be addressed.

For comparison, the images reconstructed by applying the iterative unpenalized ML-EM algorithm [1,2] to the acquired data after 20, 30, and 50 iterations are shown in Fig.2. After 20 iterations, noise and edge artifacts were present.

Fig.3 shows the images reconstructed using the penalized ML-EM algorithm to the acquired data. The Shepp-Logan filter with cutoff frequancy at half f_N was used in frequency space for the second term on the RHS of Eq.(6). The weak correlation was assumed for the first term on the RHS of Eq.(6). The top image was produced by backprojecting the filtered acquired data only (i.e., the result of FBP). The one on the second row was the initial estimate $\Phi^{(0)}$. The image on the third row was obtained after one iteration. The bottom one was the result after 9 iterations. Similar images were obtained for the Butterworth filter and the Gaussian filter. Therefore, these images are not presented here. The negative pixel values were accepted for the iteration process. Although this is not fit with the theoretical development of Eq.(5), it is interesting to see the effect on the reconstructed images (as addressed later).

The reconstructed images with the Hann filter under the same condition as described in Fig.3 are shown in Fig.4.

Fig.5 shows the reconstructed images with the Parzen filter under the same condition of Fig.3. Similar results were generated when the Lagrange filter was used. Hence, these results are not presented here.

All the frequency-space filters applied with the penalized algorithm could effectively remove the noise and edge artifacts if the frequency cutoff was properly chosen. When the cutoff frequency was set to f_N, the resulted images were noisier. If the cutoff frequency was chosen at $0.25\, f_N$, smoother images were obtained. By viewing all the horizontal and vertical profiles through the images, the Parzen filter (see Fig.5) showed the best performance on removing the artifacts among the six implemented filters. However, the Lagrange filter offers the potential to consider the detector response function. The effects of collimation variation and photon scattering may be considered via the detector response function, although the normalization factors $\{R_{ik}\}$ in Eq.(6) contain all the deterministic effects during SPECT data acquisition.

Although it is similar to the Wiener filter [25], the Lagrange filter is much easier to implement. Further study on these two filters to consider the collimation variations and photon scattering is under progress.

Since the Metz filter [26] is strongly count-dependent, it is relatively difficult to apply it in frequency space to the difference of the acquired data and the reprojected data for the iterated solution. For the initial estimate, the Metz filter has the potential to consider the effects of collimation variation and photon scattering [20].

When the iteration process generating the above images continued beyond 9 iterations, the iterated images were noisier and noisier. This instability may be due to the assumption that the correlation in image space for the first

2) The Triad SPECT system.

term $\bar{\phi}_k^{(n)}$ on the RHS of Eq.(6) is very weak. The egde-preserving smoothing [21] which reflects a relatively strong correlation was then applied to determine the first term $\bar{\phi}_k^{(n)}$. The reconstructed images using the penalized algorithm (with the six low-pass filters applied in frequency space and the edge-preserving smoothing applied in image space) were similar to the corresponding images shown above before 5 iterations. Beyond 5 iterations, the generated images were stabilized. It concludes that the edge-preserving smoothing is necessary. Under this conclusion, the smoothing in image space is consistant with that in projection space.

As an example, Figs.6 and 7 show the images obtained using the penalized algorithm with the Parzen and Lagrange filters after 10, 20, 50, and 100 iterations under the same condition as described in Fig.3, except that the first term $\bar{\phi}_k^{(n)}$ on the RHS of Eq.(6) was computed by the edge-preserving smoothing. The penalized algorithm was run up to 200 iterations. At higher iterations, only the negative pixel values changed a somewhat degree. This small effect was due to the acceptance of the negative values during iterations. It also caused small variation in the total counts of projection data after each iteration. By forcing the negative values to be zero, the iterated images after 10 iterations were similar to the 10th iterated image and the total counts after each iteration were conserved. Therefore, it is recommended that the negative pixel values are set to zero during iteration process. By forcing the negative values to be zero, the implementation of the algorithm (6) as shown above is fit with the theoretical development of Eq.(5).

V. CONCLUSIONS

We have implemented six low-pass linear filters applied in frequency space for the iterative penalized ML-EM algorithm (6). The implementation requires: (i) an edge-preserving smoothing is necessary for the first term $\bar{\phi}_k^{(n)}$ on the RHS of Eq.(6); (ii) the negative pixel values would be set to zero during iteration process. The SPECT images were reconstructed using experimentally acquired data from a chest phantom consisting of non-uniform attenuating media.

All the filters stabilized the iterated reconstructions and no stopping criterion is needed. The noise and edge artifacts associated with the ML-EM algorithm could be removed if the cutoff frequency was properly chosen. The improved performance of the Parzen and Lagrange filters relative to the others was observed. The best image, by viewing its profiles in terms of noise-smoothing, edge-sharpening, and contrast, was the one obtained with the Parzen filter. However, the Lagrange filter has the potential to consider the characteristics of detector response function.

Although the formal way of specifying an *a priori* correlation prior for the MAP solution is desired, the frequency-domain filtering approach is easier to implement. The advantage of computation will be accentuated when the effects of collimation variation and photon scattering are necessary.

VI. ACKNOWLEDGEMENT

The author is grateful to Dr. Ronald Jaszczak and Dr. Dave Gilland providing valuable comments on this paper. Mr. Kim Greer assisted with the data acquisition.

VII. REFERENCES

[1]: L. Shepp and Y. Vardi, "Maximum Likelihood Reconstruction for Emission Tomography." *IEEE Trans. Med. Imaging*, vol.1, pp.113-122, 1982.

[2]: K. Lange and R. Carson, "EM Reconstruction Algorithms for Emission and Transmission Tomography." *J. Comput. Assist. Tomog.*, vol.8, pp.306-316, 1984.

[3]: D. Snyder, M. Miller, L. Thomas and D. Politte, "Noise and Edge Artifacts in Maximum-Likelihood Reconstruction for Emission Tomography." *IEEE Trans. Med. Imaging*, vol.6, pp.228-238, 1987.

[4]: R. Hamming, *Digital Filters*, Prentice-Hall, Inc., NJ, 1983.

[5]: G. Gullberg and T. Budinger, "The Use of Filtering Methods to Compensate for Constant Attenuation in Single Photon Emission Computed Tomography." *IEEE Trans. Biomed. Engin.*, vol.28, pp.142-157, 1981.

[6]: Z. Liang, R. Jaszczak, C. Floyd, et al, "Reprojection and Backprojection in SPECT Image Reconstruction." *Proc. IEEE, Energ. Inform. Tech. Southeast*, pp.919-926, 1989.

[7]: S. Kullback and R. Leibler, "On Information and Sufficiency." *Ann. Math. Statist.*, vol.22, pp.79-86, 1951.

[8]: Z. Liang, R. Jaszczak and K. Greer, "On Bayesian Image Reconstruction from Projections: Uniform and non-uniform *a priori* source information." *IEEE Trans. Med. Imaging*, vol.8, pp.227-235, 1989.

[9]: S. Geman and D. Geman, "Stochastic Relaxation, Gibbs Distributions, and the Bayesian Restoration of Images." *IEEE Trans. Patt. Analy. Mach. Intel.*, vol.6, pp.721-741, 1984.

[10]: J. Besag, "On the Statistical Analysis of Dirth Pictures." *J. R. Statist. Soc.*, vol.48, pp.259-302, 1986.

[11]: S. Geman and D. McClure, "Statistical Methods for Tomographic Image Reconstruction." *Bull. ISI*, vol.52, pp.5-21, 1987.

[12]: R. Chin and C. Yeh, "Quantitative Evaluation of Some Edge-Preserving Noise-Smoothing Techniques." *Computer Vision, Graphics, Image Proc.*, vol.23, pp.67-91, 1983.

[13]: E. Tanaka, "A Fast Reconstruction Algorithm for Stationary Positron Emission Tomography Based on a Modified EM Algorithm." IEEE Trans. Med. Imaging, vol.6, pp.98-105, 1987.

[14]: E. Tanaka, "A Filtered Iterative Reconstruction Algorithm for Positron Emission Tomography." in *Information Processing in Medical Imaging*. Plenum Publishing Corp., pp.217-233, 1988.

[15]: E. Tanaka, "Intelligent Iterative Image Reconstruction with Automatic Noise Artifact Suppression." Presented at IEEE 1990 Medical Imaging Conference, Arlington, VA, USA.

[16]: L. Shepp and B. Logan, "The Fourier Reconstruction of a Head Section." *IEEE Trans. Nucl. Sci.*, vol.21, pp.21-43,1974.

[17]: O. Tretiak and C. Metz, "The Exponential Radon Transform." *SIAM J. Appl. Math.*, vol.39, pp.341-354, 1980.

[18]: E. Parzen, "Mathematical Considerations in the Estimation of Spectra." *Technometrics*, vol.3, pp.167-190, 1961.

[19]: D. Phillips, "A Technique for the Numerical Solution of Certain Integral Equations of the First Kind." *J. Assoc. Comput. Mach.*, vol.9, pp.84-97, 1962.

[20]: M. King, R. Schwinger, B. Penney, et al, "Digital Restoration of Indium-111 and Iodine-123 SPECT Images with Optimized Metz Filters." *J. Nucl. Medicine*, vol.27, pp.1327-1336, 1986.

[21]: Z. Liang, R. Jaszczak, C. Floyd and K. Greer, "A Spatial Interaction Model for Statistical Image Processing." in *Information Processing in Medical Imaging*. Wiley-Liss, New York, pp.29-43, 1990.

[22]: G. Gullberg, R. Huesman, J. Malko, et al, "An Attenuated Projector-Backprojector for Iterative SPECT Reconstruction." *Med. Physics*, vol.30, pp.799-815, 1985.

[23] T. Peters, "Algorithms for Fast Back-and-Reprojection in Computed Tomography." *IEEE Trans. Nucl. Sci.*, vol.28, pp.3641-3647, 1981.

[24] D. Gilland, R. Jaszczak, K. Greer and R. Coleman, "Quantitative SPECT Reconstruction of Iodine-123 Data." *J. Nucl. Medicine*, vol.31, 1991, in press.

[25]: W. Pratt, "Generalized Wiener filtering computational techniques." *IEEE Trans. Computer*, vol.21, pp.636-641, 1972.

[26]: C. Metz and R. Beck, "Quantitative Effects of Stationary Linear Image Processing on Noise and Resolution of Structure in Radionuclide Images." *J. Nucl. Medicine*, vol.15, pp.164-170, 1974.

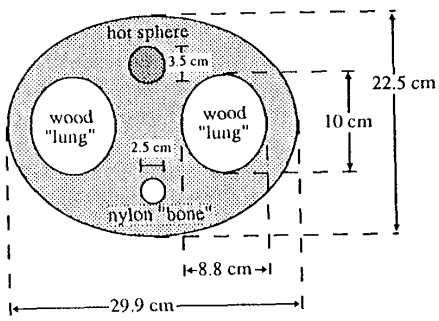

Fig.1.: The cross-section of the chest phantom.

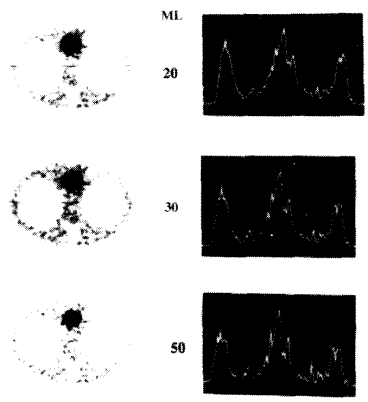

Fig.2: The images reconstructed by applying the iterative unpenalized ML-EM algorithm to the projection data acquired from the chest phantom. The top one was generated after 20 iterations. The image on the second row was obtained after 30 iterations. The bottom image was the result after 50 iterations. The curves are the profiles each through the center of the images horizontally at the indicated positions.

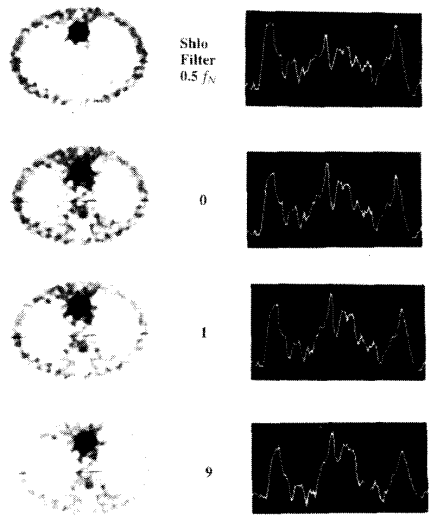

Fig.3: The images reconstructed using the penalized ML-EM algorithm with the Shepp-Logan filter at cutoff frequency of 0.5 f_N. The weak nearby correlation was assumed. The top image was produced by backprojecting the filtered projection data only. The one on the second row was the initial estimate. The image on the third row was obtained after one iteration. The bottom one was the 9th iterated result. The profiles were drawn through the images three pixels below the image center.

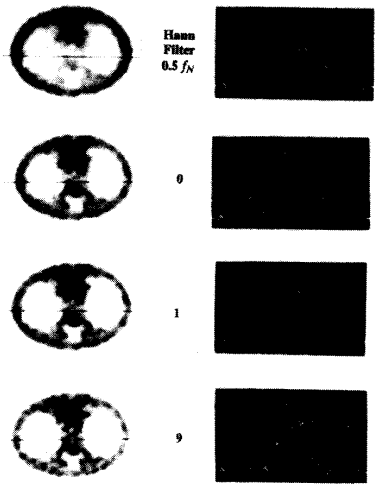

Fig.4: The reconstructed images using the penalized algorithm with the Hann filter in the same situation as described in Fig.3.

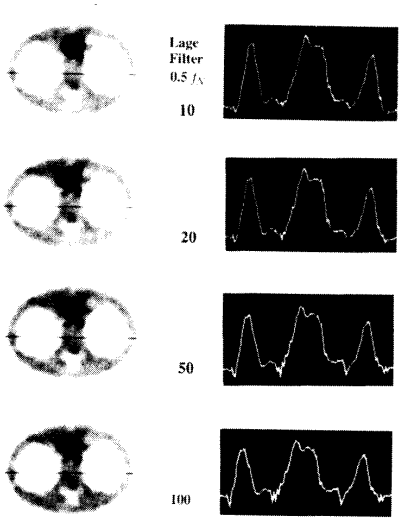

Fig.6: The images obtained using the penalized algorithm with the Parzen filter after 10, 20, 50, and 100 iterations under the same condition of Fig.3, except that the relatively strong correlation was assumed.

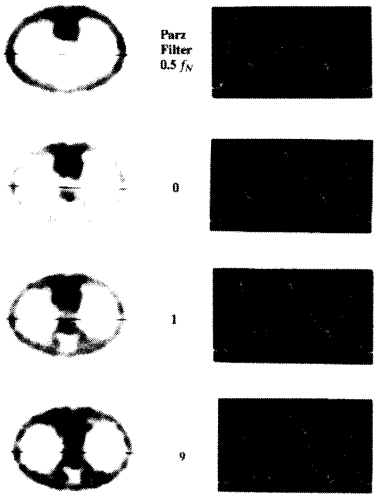

Fig.5: The reconstructed images using the penalized algorithm with the Parzen filter under the same condition of Fig.3.

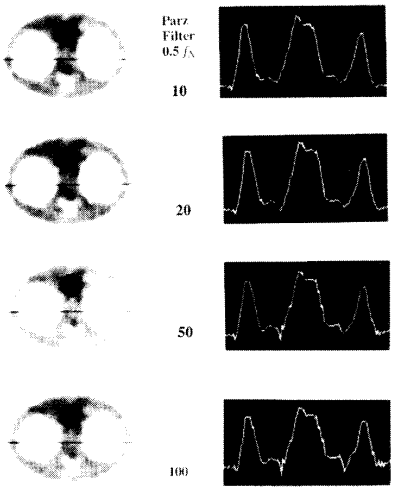

Fig.7: The images obtained using the penalized algorithm with the Lagrange filter after 10, 20, 50, and 100 iterations under the same condition of Fig.3, except that the relatively strong correlation was assumed.